Article:
Sørensen, M.E.S., Wood, A.J., Cameron, D.D. orcid.org/0000-0002-5439-6544 et al. (1 more author) (2021) Rapid compensatory evolution can rescue low fitness symbioses following partner switching. Current Biology, 31 (17). 3721-3728.e4. ISSN 0960-9822

https://doi.org/10.1016/j.cub.2021.06.034

Rapid compensatory evolution can rescue low fitness symbioses following partner-switching

Megan E S Sørensen[1], A Jamie Wood[2], Duncan D Cameron[1], Michael A Brockhurst[3*]

1. Department of Animal and Plant Sciences, University of Sheffield, Sheffield S10 2TN
2. Department of Biology, University of York, York YO10 5DD
3. Division of Evolution and Genomic Sciences, School of Biological Sciences, University of Manchester, Manchester M13 9PT

*Corresponding author Michael A. Brockhurst.
Email: michael.brockhurst@manchester.ac.uk

Summary

Partner-switching plays an important role in the evolution of symbiosis, enabling local adaptation and recovery from the breakdown of symbiosis. Because of intergenomic epistasis, partner-switched symbioses may possess novel combinations of phenotypes but may also exhibit low fitness due to their lack of recent coevolutionary history. Here, we examine the structure and mechanisms of intergenomic epistasis in the *Paramecium-Chlorella* symbiosis and test if compensatory evolution can rescue initially low fitness partner-switched symbioses. Using partner-switch experiments coupled with metabolomics we show evidence for intergenomic epistasis wherein low fitness is associated with mismatched photoprotection traits and the resulting light stress experienced by non-native symbionts when in high light environments. Experimental evolution under high light conditions revealed that an initially low fitness partner-switched non-native host-symbiont pairing rapidly adapted, gaining fitness equivalent to the native host symbiont pairing in less than 50 host generations. Compensatory evolution took two alternative routes: Either, hosts evolved higher symbiont loads to mitigate for their new algal symbiont's poor performance, or the algal symbionts themselves evolved higher investment in photosynthesis and photoprotective traits to better mitigate light stress. These findings suggest that partner-switching combined with rapid compensatory evolution can enable the recovery and local adaptation of symbioses in response to changing environments.

Keywords: Symbiosis, Experimental evolution, photosymbiosis, partner-switching

Introduction

Beneficial symbioses have an inherent potential for conflict between the symbiotic partners. This can drive the breakdown of symbiosis if environmental conditions change the net benefit of interacting or if the pursuit of individual fitness favours cheating [1]. Both situations can select for partner-switching to recombine symbiotic partnerships [2]. Partner-switching can provide hosts with access to favourable symbiotic phenotypes to overcome maladaptation to

the prevailing environmental context [3] or restore symbiont function following breakdown [4,5]. The generation of phenotypic plasticity through partner-switching arises from genetic variation of hosts (G^H) and symbionts (G^S) and intergenomic epistasis[6], that is, genetic variation for the outcome of symbiosis in the form of host genotype by symbiont genotype interactions ($G^H \times G^S$) for symbiotic traits or fitness. Furthermore, the fitness effects of symbiosis can be mediated by the environmental context [7], causing host-genotype-by-symbiont-genotype-by-environment interactions ($G^H \times G^S \times E$). A consequence of $G^H \times G^S \times E$ interactions is that there is unlikely to be an optimal host-symbiont pairing across all environments, further driving selection for partner-switching or dynamic coevolution of the symbiosis [8]. As such, partner-switching can enable niche-expansion by hosts [9,10] and provide a mechanism by which hosts can adapt to local environmental conditions faster than through *de novo* adaptation of the current symbiont [11,12].

Newly interacting partner-switched host-symbiont pairings are, however, unlikely to be co-adapted due to their lack of recent coevolutionary history and may, therefore, initially have low fitness[13–15]. Indeed, despite the adaptive potential of partner-switching, new host-symbiont pairings, like genetic mutations, may more often be deleterious than beneficial to host fitness due to phenotypic mismatches or genetic incompatibilities. This has been observed in a range of symbiotic interactions: for example, a newly acquired *Symbiodinium* endosymbiont was found to translocate less fixed carbon than the native symbiont to its cnidarian host [13]; novel bacterial endosymbionts had reduced vertical transmission rates in aphid hosts [14]; and novel *Wolbachia* endosymbionts reduced the reproductive fitness of *Drosophila simulans* [15]. How then do newly-formed, poorly co-adapted host-symbiont pairings become stable, beneficial symbioses? We hypothesise that rapid compensatory evolution (that is adaptation of the host, the symbiont, or both to ameliorate the deleterious fitness effects of partner-switching) could allow partner-switched symbioses to overcome their initially low fitness. Indeed, there is some, albeit limited, experimental evidence to support this idea: For example, the high fitness cost of newly acquired *Spiroplasma*

endosymbionts in *Drosophila melanogaster* was ameliorated within only 17 host generations[16], although the underlying mechanisms of this fitness recovery remain unknown. Furthermore, horizontal gene transfers were found to have caused the rapid evolution of nonsymbiotic strains of rhizobia bacterial symbionts into symbiotic partners in field-site tests with *Lotus* plant hosts[17].

The microbial symbiosis between *Paramecium bursaria* and *Chlorella* provides an experimentally tractable model system to study intergenomic epistasis and the underlying molecular mechanisms. The ciliate host, *P. bursaria*, is a single-celled eukaryote, and each host cell contains 100-600 cells of the algal endosymbiont, *Chlorella* [18,19]. The *P. bursaria* - *Chlorella* symbiosis is based on a primary nutrient exchange of fixed carbon from the photosynthetic alga for organic nitrogen from the heterotrophic host [18,20]. *Chlorella* algal symbionts are primarily vertically transmitted to daughter cells at *Paramecium* cell division, although additional algal symbionts can also be acquired from the environment by ingestion[21,22]. This symbiosis is geographically widespread and genetically diverse, in part due to multiple independent acquisitions of algal symbionts by *P. bursaria*. The primary nutrient exchange is convergent among these origins, facilitating partner-switching, with concurrent divergence in other metabolic traits, causing phenotypic mismatches in partner-switched host-symbiont pairings [23]. Here, using experimental partner-switches, we examined the pattern and mechanisms of intergenomic epistasis for three diverse host-symbiont strains, observing significant $G^H \times G^S \times E$ interactions for host-symbiont growth rate and symbiont load (that is the number of symbionts per host cell), together with corresponding differences in metabolism. We then experimentally evolved a low fitness partner-switched host-symbiont pairing for ~50 host generations. We observed rapid compensatory evolution by hosts and symbionts that improved fitness to equal to that of the native host-symbiont pairing mediated by evolved changes in host control of symbiont load and in symbiont metabolism.

Results and Discussion

Intergenomic epistasis for host-symbiont growth and symbiont load. We constructed all possible host-symbiont genotype pairings (n = 9) of 3 diverse strains of *Paramecium-Chlorella* and confirmed their identity by diagnostic PCR (Figure S1). We measured the growth reaction norm of each host-symbiont pairing across a light gradient (Figure 1a). All host-symbiont pairings showed the classic photosymbiotic reaction norm [24], such that growth rate increased with irradiance, but we observed a significant $G^H \times G^S \times E$ interaction for host-symbiont growth rate ($G^H \times G^S \times E$ interaction, ANOVA, $F_{17,162} = 18.81$, $P<0.001$) consistent with intergenomic epistasis. This was driven by contrasting effects of symbiont genotype on growth in the different host backgrounds across light environments. In the HK1 and HA1 host-backgrounds, similar growth reaction norms with light were observed for each symbiont genotype, whereas in the 186b host background the growth reaction norm varied according to symbiont genotype. Interestingly, the native 186b host-symbiont pairing had both the lowest intercept and the highest slope, indicating that in the 186b host background the native algal symbiont genotype was costlier in the dark yet more beneficial in high-light environments than non-native algal symbiont-genotypes.

P. bursaria host cells regulate their algal symbiont load (i.e. the number of symbionts per host cell) according to light irradiance to maximise the benefit-to-cost ratio of symbiosis, such that, for naturally occurring host-symbiont pairings, symbiont load peaks at intermediate irradiance and is reduced both in the dark and at high irradiance [24–26]. To test if regulation of symbiont load varied among host-symbiont pairings, we measured symbiont load across the light gradient as the intensity of single-cell fluorescence, which is correlated with the number of symbionts per host cell[19], by flow cytometry (Figure 1b). All host-symbiont pairings showed the expected unimodal symbiont load curve with light, but nevertheless we observed a significant $G^H \times G^S \times E$ interaction for symbiont load ($G^H \times G^S \times E$ interaction, ANOVA, $F_{17,162} = 3.78$, $P<0.001$) consistent with intergenomic epistasis. Whereas, in the HA1 host similar symbiont load reaction norms were observed for each

symbiont genotype, for the HK1 and 186b host backgrounds the form of the symbiont load reaction norms varied according to symbiont genotype. In the HK1 host, the magnitude of the symbiont load varied by symbiont genotype, such that higher symbiont loads were observed for the native compared to the non-native symbiont-genotypes. In the 186b host, peak symbiont load occurred at different light levels according to symbiont genotype, such that for the native symbiont the symbiont load curve peaked at a higher light intensity when compared to the non-native symbionts. (For the full output of the polynomial model, see Table S1.) Because symbiont load is primarily host-controlled in this system[24,25], this suggests that the HK1 and 186b host-genotypes discriminated among symbiont-genotypes, and then regulated symbiont load accordingly.

Metabolic mechanisms of intergenomic epistasis. To investigate the potential metabolic mechanisms underlying the observed intergenomic epistasis we performed untargeted global metabolomics with ESI-ToF-MS independently for the host and symbiont metabolite fractions for each host-symbiont pairing across the light gradient [23]. Light irradiance was the primary driver of differential metabolism for both host and symbiont, however, host-dependent differences in the metabolism of symbiont-genotypes could be detected. For the symbiont metabolite fraction subset by host-genotype, we observed native versus non-native clustering of symbiont metabolism only when associated with the 186b host-genotype (Figure S2). This is consistent with the larger phenotypic differences in growth and symbiont load observed among host-symbiont pairings with the 186b host-genotype compared to with either the HK1 or HA1 host-genotypes. We therefore focused our analyses on comparing the metabolic profiles of the different symbiont genotypes within the 186b host background. Pairwise contrasts of the symbiont-genotypes in the 186b host-genotype background revealed a range of candidate symbiont metabolites which distinguished the native pairing from either non-native host-symbiont pairing. Putative identifications included, in the dark, elevated levels of candidate metabolites associated with stress responses (stress-associated hormones, jasmonic acid and abscisic acid, and stress associated-fatty acids,

such as arachidonic acid) but reduced production of vitamins and co-factors by the native symbiont, compared to the non-native symbionts (Table S2). At high irradiance, the native symbiont showed higher levels of candidate metabolites in central metabolism, hydrocarbon metabolism and of biotin (vitamin B7), compared to the non-native symbionts (Table S2). In contrast, the non-native symbionts produced elevated levels, relative to native symbionts, of a candidate glutathione derivative; glutathione is an antioxidant involved in the ascorbate-glutathione cycle that combats high UV stress through radical oxygen scavenging [27,28]. Together, these data suggest that intergenomic epistasis was associated with mismatches in photoprotection and consequent responses to light stress by symbionts in non-native host-symbiont pairings.

Rapid compensatory evolution can rescue an initially low fitness partner-switched symbiosis. The partner-switched pairing of the 186b host with the HK1 symbiont showed substantially reduced growth at high light relative to the native 186b host-symbiont pairing. To test if this fitness deficit could be overcome through compensatory evolution, we established six replicate populations of each of these two symbiotic partnerships (i.e., the 186b host with the 186b algal symbiont and the 186b host with the HK1 algal symbiont), which were propagated by weekly serial transfer for 25 transfers (approximately 50 host generations) at a high light regime (50µE; 14:10 L:D). The growth rate per transfer was higher for the native pairing than the non-native pairing (Figure S3a) (linear mixed effect model, HK1 symbiont fixed effect of -0.08 ±0.006, T-value = -14.126, see Table S1 for full statistical output), but increased over time for both pairings (transfer number fixed effect 0.001 ±0.0004, T-value = 3.088). To test for adaptation, we compared the fitness effect of symbiosis at the beginning and the end of the transfer experiment by direct competition of either the ancestral or evolved host-symbiont pairings against the symbiont-free ancestral 186b host genotype across a light gradient. Fitness at the start of the evolution experiment of symbiotic relative to non-symbiotic hosts increased more steeply with irradiance for the native than the partner-switched non-native pairing (Figure 2), but this difference had

disappeared by the end of the evolution experiment, such that both the native and non-native host-symbiont pairings showed increasing fitness relative to non-symbiotic hosts with increasing irradiance (symbiont genotype by light intensity by transfer number interaction term: ANOVA, $F_{7,45}$ =6.20, P<0.001). Indeed, at 50 µE m^{-2} s^{-1}, the light level used in the selection experiment, the large fitness deficit observed between the native and non-native pairing at the beginning of the experiment had been completely compensated. Comparison of the growth reaction norms of the evolving populations over time suggested that this amelioration occurred rapidly: By the tenth transfer, the native and non-native host-symbiont pairings showed equivalent growth responses to light (Welch t-test t(45.96) = -0.26, p = 0.80), in contrast to their substantially different ancestral growth reaction norms observed at the start of the evolution experiment (Welch t-test t(35.79) = 3.59, p = <0.001) (Figure S3b). These data suggest that newly established partner-switched symbioses can rapidly achieve equivalent growth performance and fitness benefits as the native host-symbiont pairing by compensatory evolution.

Evolved changes in symbiont load regulation and metabolism. To understand the mechanisms of compensatory evolution, we first compared the symbiont load reaction norms of the ancestral and evolved native and non-native pairings (Figure 3). Both ancestral host-symbiont pairings showed the expected unimodal symbiont load curve with light, albeit with higher symbiont loads for the native compared to the non-native pairing at the highest light level, 50 µE m^{-2} s^{-1} irradiance, as used in the transfer experiment. By the end of the evolution experiment, the shape of the symbiont load reaction norms were altered in both the native and non-native pairings. Most notably, at 50 µE m^{-2} s^{-1} irradiance, whereas the non-native pairing had increased symbiont load, symbiont load had decreased in the native pairing, such that symbiont load was now higher in the non-native pairing (transfer by symbiont genotype interaction at high light: ANOVA, $F_{3,20}$ = 16.88, P<0.001). Higher symbiont loads may therefore have contributed to the observed increased fitness of evolved compared to ancestral non-native pairings in the high light environment.

Next, to investigate the potential underlying metabolic mechanisms, we performed untargeted metabolomics analyses on the separated *Chlorella* and *P. bursaria* fractions from samples taken the start and end of the evolution experiment grown at 50 µE m^{-2} s^{-1}. The ancestral *P. bursaria* and *Chlorella* metabolic profiles of native and non-native host-symbiont pairings could be clearly distinguished (Figure 4). At the end of the evolution experiment, *P. bursaria* metabolism displayed a high degree of apparent convergence between hosts evolved with the native versus the non-native symbionts (Figure 4a,c). This was driven by decreased levels of compounds of central metabolism (such as pyruvate and TCA cycle intermediates, antioxidants, lipids, and some amino acids) (Table S3), suggesting either increased pathway completion or a reduced metabolic rate, both of which can lead to increased efficiency. In addition, we observed increased levels of the amino acid cysteine and a shikimate pathway component in hosts evolved with the native versus the non-native symbionts (Figure S4). Levels of algal-cell degradation components (Figure S4), such as cell-wall degradation product chitotriose, were increased in some replicates of hosts evolved with either symbiont, potentially suggesting increased digestion of *Chlorella*, which is a known mechanism by which hosts control their symbiont load [29,30].

In contrast, evolved changes to the metabolic profiles of the algal symbiont genotypes showed less consistent differences among treatments (Figure 4b,d). Whereas all replicates of the native 186b *Chlorella* evolved in a similar direction, the replicates of the non-native HK1 *Chlorella* evolved in two different directions. Two of the HK1 replicates took a similar trajectory to the 186b symbionts, while the remaining four replicates all followed an alternative evolutionary trajectory. The group of four HK1 replicates that diverged during the experiment had lower production of metabolites within core aspects of metabolism, such as lipids, amino acids and carbohydrates. The second group, including the remaining two HK1 replicates and all the 186b replicates, had for the most part higher production of metabolites within primary metabolism pathways, particularly within lipids and carbohydrates, as well as

a key chlorophyll compound, a photo-protective carotenoid (though not for all of the 186b replicates), and secondary metabolites with potential antioxidant properties (Figure S4, Table S3). This greater investment into photosynthesis and photo-protection may improve carbon transfer to the host [31,32], and decrease light stress, which aligns with the decrease in host antioxidants. Interestingly, the two HK1 replicates that appeared to converge metabolically with the native symbionts had a lower increase in symbiont load compared to the replicates that metabolically diverged (Table S4). This implies that the evolution of metabolism and symbiont load were linked, and that overall two alternative strategies of compensatory evolution emerged: either to have fewer, more beneficial symbionts or to have more, less-beneficial symbionts.

Conclusion

Partner switching plays an important role in the evolution of a wide range of symbioses [2,4,5,33,34] enabling adaptation to changing environments and recovery from the breakdown of symbiosis. Because of intergenomic epistasis, partner-switched host-symbiont pairings may possess novel adaptive phenotypes, but will sometimes exhibit low fitness associated with mismatches between host and symbiont traits, owing to their lack of recent coevolutionary history [14,15,35]. In the *Paramecium-Chlorella* symbiosis, low fitness following partner switching was associated with mismatching putative photoprotection traits and the resulting light stress experienced by non-native symbionts when in high light environments. This corresponds with findings from other photosynthetic symbioses, including coral-*Symbiodinium* and *Hydra-Chlorella*, where mismatching thermal and light stress tolerances contribute to the breakdown of symbiosis [36–39]. Low fitness, partner-switched host-symbiont pairings were rescued by compensatory evolution, which took one of two routes: Either, hosts evolved higher symbiont loads to mitigate for their new algal symbiont's poor performance, or the algal symbionts themselves evolved higher investment in photosynthesis and photoprotection traits to better mitigate light stress. Given that symbiont load varies with light due to host control[24,25], it seems likely that the evolved change in symbiont load is due to

phenotypic plasticity through altered host regulation, whereas the evolved change in algal photosynthetic metabolism could be due to either genetic or physiological adaptation by the symbionts. Both strategies increased growth of the non-native host-symbiont pairing, leading to higher fitness equivalent to that of the native host-symbiont pairing. Together, these data suggest that, partner-switching combined with rapid compensatory evolution can contribute to the recovery of symbiosis and local adaptation of hosts to changing environmental conditions. Partner-switching combined with rapid compensatory evolution could thus enhance the resilience of symbioses to environmental change, enabling the maintenance of their contribution to ecosystem function. Moreover, the potential fitness benefits of the phenotypic plasticity provided by partner-switching may select against the evolution of strict vertical transmission in symbioses that inhabit fluctuating or rapidly changing environments.

Acknowledgements

This work was funded by grants NE/K011774/2 and NE/V000128/1 from the Natural Environment Research Council, UK to M.A.B, D.D.C, and A.J.W and a White Rose DTP studentship from the Biotechnology and Biological Sciences Research Council, UK (BB/011151/1) to M.E.S.S. The funders had no role in the design of the study, the collection, analysis and interpretation of data or writing of the manuscript. We are grateful to Heather Walker for her technical assistance with the mass spectrometry.

Author Contributions: M.A.B, D.D.C, and M.E.S.S conceived and designed the study. M.E.S.S conducted experimental work. M.E.S.S and D.D.C analysed the data. M.E.S.S and M.A.B drafted the manuscript. All authors commented on the manuscript.

Competing Interest Statement: The authors declare no conflict of interests.

Figure Legends

Figure 1. Intergenomic epistasis of host symbiont growth rate and symbiont load reaction norms. For both A and B, each panel presents the data for a specific genotype of *P. bursaria* host, as indicated at top of each panel, and the symbiont genotypes are distinguished by colour. A) Initial growth rates of the host-symbiont pairings across a light gradient over three days. The data points show the mean (n=3) initial growth rate ±SE. The host-symbiont growth rate reaction norm varied by symbiont genotype in the 186b host genotype but did not vary in the HA1 or HK1 host genotypes, consistent with intergenomic epistasis. B) Symbiont load of the host-symbiont pairings across a light gradient. The data points show the mean (n=3) symbiont load, measured as relative chlorophyll fluorescence, ±SE. The lines show polynomial models; the model coefficients showed a significant G^H x G^S interaction (ANOVA, $F_{8,36}$ =27.22 (the intercept); 8.58 (first coefficient); 6.09 (second coefficient), $P<0.001$). For full statistical output see Table S1. The symbiont load reaction norm varied by symbiont genotype in both the HK1 and 186b host genotypes but did not vary in the HA1 host genotype, consistent with intergenomic epistasis.

Figure 2. Relative fitness reaction norms at the start and end of the evolution experiment. Panels show relative fitness reaction norms across a light gradient of various host-symbiont pairings in the 186b host genotype in direct competition with the symbiont-free 186b host genotype. The left-hand panel shows fitness reaction norms measured at the start of the evolution experiment (T0) and the right-hand panel shows fitness reaction norms measured at the end of the evolution experiment (T25), as indicated at the top of each panel. Relative fitness was calculated as the selection rate, where a value above 0 indicates a fitness benefit to the host of carrying algal symbionts. Colours show the symbiont genotype treatment, where blue denotes that the 186b host carried the native 186b symbiont genotype whereas grey denotes that the 186b host carried the non-native HK1 symbiont genotype. Dark, thick lines show the mean (n=6) relative fitness reaction norms and light, thin lines show the relative fitness reaction norms for each individual replicate. At the start of the evolution experiment only the native host-symbiont pairing showed an increasing fitness benefit of carrying symbionts with increasing irradiance, whereas at the end of the evolution experiment both the native and non-native host symbiont pairings showed an increasing fitness benefit of carrying symbionts with increasing irradiance.

Figure 3. Symbiont load reaction norms at the start and end of the evolution experiment. Panels show symbiont load reaction norm across a light gradient of various host-symbiont pairings in the 186b host genotype. The left-hand panel shows symbiont load reaction norms measured at the start of the evolution experiment (T0) and the right-hand panel shows symbiont load reaction norms measured at the end of the evolution experiment (T25), as indicated at the top of each panel. Colours show the symbiont genotype treatment, where blue denotes that the 186b host carried the native 186b symbiont genotype whereas grey denotes that the 186b host carried the non-native HK1 symbiont genotype. Symbols show the mean (n=6) ± standard error symbiont load and lines show the symbiont load reaction norms for each individual replicate. At the irradiance level used in the evolution experiment (50 µE m^{-2} s^{-1}), we observed that whereas mean symbiont load of the native symbiont had reduced, symbiont load of the non-native symbiont had increased, by the end of the evolution experiment.

Figure 4. Evolutionary trajectories of *Paramecium* and *Chlorella* metabolism. Panels A and C show PCA plots for *P. bursaria* metabolism, while panels B and D show PCA plots for *Chlorella* metabolism, as indicated in the panel labels. The top row (A and B) plot PC1 versus PC2. The bottom row (C and D) plot PC2 versus PC3. The percent variation explained by each PC is shown on the associated axis label. Colours show the symbiont genotype treatment, where blue denotes that the 186b host carried the native 186b symbiont genotype whereas grey denotes that the 186b host carried the non-native HK1 symbiont genotype. Dark points show ancestral metabolism at the state of the evolution experiment (mean of n=6) whereas light points show the metabolism of each individual replicate population at the end of the evolution experiment (mean of n=3 technical replicates per population). Arrows show the trajectory of metabolic evolution followed by each replicate population during the evolution experiment, and 95% confidence ellipses have been drawn for each treatment. The metabolite identifications for the top loadings are shown in their corresponding location. Related to Table S3 and Figure S4.

STAR Methods

Resource availability

Lead contact

Further information and requests for resources and reagents should be directed to and will be fulfilled by the Lead Contact, Michael Brockhurst (michael.brockhurst@manchester.ac.uk). The natural strains used in this paper are available from culture collections (see below), unfortunately all our experimental populations were lost during the lab closures at the beginning of the global Covid pandemic.

Materials availability

This study did not generate new unique reagents.

Data and code availability

The data has been deposited within Mendeley Data (DOI: 10.17632/m7tpzttyjx.1).

Experimental Model and Subject Details

The three natural strains of symbiotic *P. bursaria* used were: 186b (CCAP 1660/18) obtained from the Culture Collection for Algae and Protozoa (Oban, Scotland), and HA1 and HK1 isolated in Japan and obtained from the Paramecium National Bio-Resource Project (Yamaguchi, Japan). *P. bursaria* stock cultures were maintained at 25^{o}c under a 14:10 L:D cycle with 50 µE m^{-2} s^{-1} of light (a hight light condition). The stocks were maintained by batch culture in bacterized Protozoan Pellet Media (PPM, Carolina Biological Supply), made to a concentration of 0.66 g L^{-1} with Volvic natural mineral water, and inoculated approximately 20 hours prior to use with *Serratia marscesens* from frozen glycerol stocks.

To isolate *Chlorella* from the symbiosis, symbiotic cultures were first washed and concentrated with a 11µm nylon mesh using sterile Volvic. The suspension was then ultrasonicated using a Fisherbrand™ Q500 Sonicator (Fisher Scientific, NH, USA), at a power setting of 20% for 10 seconds sonification to disrupt the host cells. The liquid was then spotted onto Bold Basal Media plates (BBM) [40], from which green colonies were

streaked out and isolated over several weeks. Plate stocks were maintained by streaking out one colony to a fresh plate every 3/4 weeks.

Symbiont-free *P. bursaria* were made by treating symbiotic cultures with paraquat (10 µg mL^{-1}) for 3 to 7 days in high light conditions (>50 µE m^{-2} s^{-1}), until the host cells were visibly symbiont free. The cultures were then extensively washed with Volvic and closely monitored with microscopy and flow cytometry over a period of several weeks to check that re-greening by *Chlorella* did not occur. Stock cultures of the symbiont-free cells were maintained by batch culture at 25ºc under a 14:10 L:D cycle with 3 µE m^{-2} s^{-1} of light and were given fresh PPM weekly. Symbiont-free *Paramecium* stocks have been maintained for a substantial period of time (months/years) without *Chlorella* ever being observed either inside or outside of *Paramecium* cells. In addition, using flow cytometry we have never observed chlorophyll fluorescence for *Paramecium* cells sampled from these stocks (methodology detailed in symbiont Load section). Together these tests confirms that paraquat treatment successfully removes all of the native *Chlorella*.

Method Details

Cross infection

Symbiont-free populations of the three *P. bursaria* strains were re-infected by adding a colony of *Chlorella* from the plate stocks derived from the appropriate strain. This was done with all three of the isolated *Chlorella* strains to construct all possible host-symbiont genotype pairings (n=9). The regreening process was followed by microscopy and took between 2-6 weeks. Over the process, cells were grown at the intermediate light level of 12 µE m^{-2} s^{-1} and were given bacterized PPM weekly.

Diagnostic PCR

The correct algae genotype within the cross-infections was confirmed using diagnostic PCR. The *Chlorella* DNA was extracted by isolating the *Chlorella* and then using a standard 6% Chelex100 resin (Bio-Rad) extraction method. A nested PCR technique with overlapping, multiplex Chlorophyta specific primers were used as described by Hoshina et al. [41]. Standard PCR reactions were performed using Go Taq Green Master Mix (Promega) and 0.5µmol L^{-1} of the primer. The thermocycler programme was set to: 94ºc for 5min, 30 cycles of (94ºc for 30sec, 55ºc for 30sec, 72ºc for 60sec), and 5 min at 72ºc.

Growth rate

Growth rates of the host-symbiont pairings were measured across a light gradient. The cells were washed and concentrated with a 11µm nylon mesh using sterile Volvic and re-suspended in bacterized PPM. The cultures were then split and acclimated to their treatment light condition (0, 12, 24, & 50 µE m^{-2} s^{-1}) for five days. The cultures were then re-suspended in bacterized PPM to a target cell density of 150 cell mL^{-1}. Cell densities were measured at 0, 24, 48 and 72 hours by fixing 360µL of each cell culture, in triplicate, in 1% v/v glutaraldehyde in 96-well flat-bottomed micro-well plates. Images were taken with a plate reader (Tecan Spark 10M) and cell counts were made using an automated image analysis macro in ImageJ v1.50i [42]. The initial host-symbiont growth rate was measured over a period of three days.

Symbiont load

The symbiont load (i.e., the number of symbionts per host cell) was measured in cultures derived from the growth rate experiment so that the data could be integrated between the two measurements. Triplicate 300µl samples of each cell culture were taken from 72-hour cultures for flow cytometry analysis. Host symbiont load was estimated using a CytoFLEX S flow cytometer (Beckman Coulter Inc., CA, USA) by measuring the intensity of chlorophyll fluorescence for single *P. bursaria* cells (excitation 488nm, emission 690/50nm) and gating cell size using forward side scatter; a method established by Kadono et al. [19]. The measurements were calibrated against 8-peak rainbow calibration particles (BioLegend), and then presented as relative fluorescence to reduce variation across sampling sessions.

Partner-switching - Metabolomics

Cultures of the host-symbiont pairings were washed and concentrated with a 11µm nylon mesh using sterile Volvic and re-suspended in bacterized PPM. The cultures were then split and acclimated at their treatment light condition (0, 12 & 50 µE m^{-2} s^{-1}) for seven days. The symbiotic partners were separated in order to a get *P. bursaria* and *Chlorella* metabolic fraction. The *P. bursaria* cells were concentrated with a 11µm nylon mesh using Volvic and then the *P. bursaria* cells were disrupted by sonication (20% power for 10 secs). 1ml of the lysate was pushed through a 1.6µm filter, which caught the intact *Chlorella* cells, and the run-through was collected and stored as the *P. bursaria* fraction. The 1.6µm filter was washed with 5ml cold deionized water, and then reversed so that the *Chlorella* cells were resuspended in 1ml of cold methanol, which was stored as the *Chlorella* fraction. After which the *Chlorella* fraction samples were already in methanol, but the *P. bursaria* fraction samples had then to be diluted by 50% with methanol.

Metabolic profiles were recorded using ESI ToF-MS, on the Qstar Elite with automatic injection using Waters Alliance 2695 HPLC (no column used), in positive mode. This is an established high-throughput method with a large mass range (50 Da to 1000 Da).

Mass spectrometry settings:

Polarity:	positive
Ion Spray voltage:	4.2 kV
Declustering potential:	120 V
Focusing potential:	265 V
Source temperature:	200°c
Gas Flow:	40 ml min^{-1}
Solvent:	50:50 methanol to water at flow rate 40µl min^{-1}
Injected volume:	10µl

The processing was performed using in-house software Visual Basic macro 216 [43], which combined the spectra across the technical replicates by binning the crude m/z values into 0.2-unit bins. The relative mass abundances (% total ion count) for each bin was summed. Pareto scaling was applied to the results, and the data was then analysed by principal component analysis using SIMCA-P software (Umetrics). When treatment-based separation was observed, supervised orthogonal partial least squares discriminant analysis (OPLS-DA) separation was then performed using the discriminatory treatment with the SIMCA-P software.

Partner-switching - Identification of significant masses

Masses of interest were annotated using the initial identifications from the in-house software program and further comparisons against KEGG (https://www.genome.jp/kegg/) [44,45] and Metlin (https://metlin.scripps.edu) [46] databases. The Metabolomics Standards Initiative requires two independent measures to confirm identity, this partner-switching metabolomic analysis only used one measure (accurate mass) and therefore, meets only the level 2 requirements of putative annotated compounds.

Evolution Experiment

The populations used derive from the cross-infections and, therefore, the host-symbiont pairings come from the same cured 186b ancestor that was then re-infected with either its native (186b) or non-native (HK1) symbionts. The two host-symbiont pairings were split into six replicate populations that were used as the starting populations. The 200ml populations were propagated by weekly serial transfer for 25 transfers at a high light

(50 µE m^{-2} s^{-1}) 14:10 L:D cycle. At every transfer, cell-density was equalised to 100 cells mL^{-1} and the transferred cells were washed with a 11µm nylon mesh using Volvic before being re-suspended in bacterized PPM. Cell density was measured before and after each transfer by fixing 360µL of each cell culture, in triplicate, in 1% v/v glutaraldehyde in 96-well flat-bottomed micro-well plates. Images were taken with a plate reader (Tecan Spark 10M) and cell counts were made using an automated image analysis macro in ImageJ v1.50i [42]. Growth rate and symbiont load assays were conducted at the start, T10, T20 and end of the experiment using the method described above.

Evolution experiment - Fitness assay

Fitness assays were conducted at the start and end of the evolution experiment. *P. bursaria* cultures, both the symbiotic pairings and the symbiont-free ancestor, were washed with Volvic and resuspended in bacterized PPM. The cultures were then split and acclimated at their treatment light level (0,12,50 µE m^{-2} s^{-1}) for five days. Cell densities were counted by fixing 360µL of each cell culture, in triplicate, in 1% v/v glutaraldehyde in 96-well flat-bottomed micro-well plates. Images were taken with a plate reader (Tecan Spark 10M) and cell counts were made using an automated image analysis macro in ImageJ v1.50i [42]. The competitions were started by setting up microcosms that each contained 50:50 populations of green and white cells (with target values of 20 green cells and 20 white cells per mL) that were in direct competition. Cells were sampled on day 0 and day 7 on a flow cytometer and the proportion of green to white cells was measured and used to calculate the selection rate. Selection rate (R) is calculated as the difference in Malthusian parameters of green (test) versus white (reference) cell populations in direct competition: $R = (\ln(test_{start}/test_{end}) - \ln(reference_{start}/reference_{end}))$ / day [47]. Green versus white cells were distinguished using single cell fluorescence estimated using a CytoFLEX S flow cytometer (Beckman Coulter Inc., CA, USA) by measuring the intensity of chlorophyll Fluorescence (excitation 488nm, emission 690/50nm) and gating cell size using forward side scatter; a method established by Kadono et al. [19]. The measurements were calibrated against 8-peak rainbow calibration particles (BioLegend), and then presented as relative fluorescence to reduce variation across sampling sessions. The re-establishment of endosymbiosis takes between 2-4 weeks, and this method was tested to ensure that the symbiont-free cells do not re-green over the course of the experiment.

Evolution experiment - Metabolomics

The cultures were sampled at the start and end of the evolution experiment. Cultures were washed and concentrated with a 11µm nylon mesh using Volvic and re-suspended in bacterized PPM. The cultures were acclimated at their treatment light condition (50 µE m^{-2} s^{-}

[1]) for seven days. At the start of the evolution experiment we analysed a sample from each of the 6 replicate populations per treatment to determine the ancestral metabolomes of each host-symbiont pairing (i.e., n=6). At the end of the evolution experiment, we increased our replication such that for each of the 6 replicate populations per treatment we analysed 3 technical replicates, allowing us to determine differences between replicate populations as well as between treatments in their evolved metabolomes. At each sampling event, the symbiotic partners were separated in order to a get *P. bursaria* and *Chlorella* metabolic fraction using the extraction method described above. Samples were freeze-dried for storage, and then resuspended in 50:50 methanol to water prior to mass spectrometry.

The samples were analysed with a Synapt G2-Si with Acuity UPLC, recording in positive mode over a large untargeted mass range (50 – 1000 Da). A 2.1x50mm Acuity UPLC BEH C18 column was used with acetylnitrile as the solvent. The machine settings are listed in detail below:

Mass spectrometry settings:

Polarity:	positive
Capillary voltage:	2.3 kV
Sample Cone voltage:	20 V
Source Temperature:	100^{o}c
Desolvation temperature:	280^{o}c
Gas Flow:	600 L hr^{-1}
Injected volume:	5µl
Column temperature:	45^{o}c

Gradient information:

Time (mins)	Water (%)	Acetonitrile (%)
0	95	5
3	65	35
6	0	100
7.5	0	100
7.6	95	5

The *P. bursaria* and *Chlorella* fraction were analysed separately. The xcms R package [48–50] was used to extract the spectra from the CDF data files, using a step argument of 0.01 m/z. Peaks were identified, and then grouped across samples. These aligned peaks were used to identify and correct correlated drifts in retention time from run to run. Pareto scaling was applied to the resulting intensity matrix.

Evolution experiment - Metabolomics analysis

The metabolic profiles from the start and end of the experiment were compared using principal component analysis (PCA) with the prcomp() function in Base R (https://www.rproject.org/). For both fractions the first three components were considered, this accounted for >88% of the variance. The top 1% of the loadings were selected using the absolute magnitude of the loadings. These top loadings were identified where possible, and the identified loadings were then depicted in their associated component space. The relative abundance of these top loadings was visualised using heatmaps drawn with the heatmap.2() function from the gplot package [51]. The phylogenies were based on UPGMA clustering of the PCA coordinates of the samples using the hclust() function. This approach of integrating metabolic data and genotypes in heatmaps has been used previously [52].

Evolution experiment - Identification of significant masses

Masses of interest were investigated using the MarVis-Suite 2.0 software (http://marvis.gobics.de/) [53], using retention time and mass to compare against KEGG (https://www.genome.jp/kegg/) [44,45] and MetaCyc (https://biocyc.org/) [54] databases. The Metabolomics Standards Initiative requires two independent measures to confirm identity, which the combination of retention time and accurate mass achieves for the analysis of the evolution experiment metabolomics.

Quantification and Statistical analysis

Statistical analyses were performed in Rv.3.5.0 [55] and all plots were produced using package ggplot2 [56] unless otherwise stated. Physiology tests were analysed by both ANOVA and ANCOVA, with transfer time, host and symbiont identity as factors. A linear mixed effect model was used to analysis the growth rate per transfer using lm() function from the nlme package [57]. The lm model included fixed effects of symbiont genotype and transfer number, and random effects of transfer number given sample ID. Where parametric tests were used the data conformed to parametric assumptions of independence, normality and homogeneity of variance, which was confirmed using the appropriate tests and plots (e.g normal QQ and residual vs fitted values). Summary details of the data is provided in the figure legends (e.g the value of n and type of error used) and details of the statistical methods used are within the supplementary statistics table (Table S1).

Supplementary excel table

Table S1. Statistical outputs for analyses associated with the figures of the main manuscript and supplementary figures. Related to Figures 1A, 1B, 2, 3, & S3.

References:

1. Sachs, J.L., and Simms, E.L. (2006). Pathways to mutualism breakdown. Trends in Ecology & Evolution *21*, 585–592.

2. Boulotte, N.M., Dalton, S.J., Carroll, A.G., Harrison, P.L., Putnam, H.M., Peplow, L.M., and van Oppen, M.J. (2016). Exploring the *Symbiodinium* rare biosphere provides evidence for symbiont switching in reef-building corals. The ISME Journal *10*, 2693–2701.

3. Lefèvre, C., Charles, H., Vallier, A., Delobel, B., Farrell, B., and Heddi, A. (2004). Endosymbiont Phylogenesis in the Dryophthoridae Weevils: Evidence for Bacterial Replacement. Mol Biol Evol *21*, 965–973.

4. Koga, R., and Moran, N.A. (2014). Swapping symbionts in spittlebugs: evolutionary replacement of a reduced genome symbiont. The ISME Journal *8*, 1237–1246.

5. Matsuura, Y., Moriyama, M., Łukasik, P., Vanderpool, D., Tanahashi, M., Meng, X.-Y., McCutcheon, J.P., and Fukatsu, T. (2018). Recurrent symbiont recruitment from fungal parasites in cicadas. PNAS *115*, E5970–E5979.

6. Heath, K.D. (2010). Intergenomic Epistasis and Coevolutionary Constraint in Plants and Rhizobia. Evolution *64*, 1446–1458.

7. Thompson, J.N. (2005). The Geographic Mosaic of Coevolution (University of Chicago Press).

8. Heath, K.D., and Tiffin, P. (2007). Context dependence in the coevolution of plant and rhizobial mutualists. Proceedings of the Royal Society of London B: Biological Sciences *274*, 1905–1912.

9. Joy, J.B. (2013). Symbiosis catalyses niche expansion and diversification. Proceedings of the Royal Society B: Biological Sciences *280*, 20122820.

10. Sudakaran, S., Kost, C., and Kaltenpoth, M. (2017). Symbiont Acquisition and Replacement as a Source of Ecological Innovation. Trends in Microbiology *25*, 375–390.

11. Jaenike, J., Unckless, R., Cockburn, S.N., Boelio, L.M., and Perlman, S.J. (2010). Adaptation via Symbiosis: Recent Spread of a Drosophila Defensive Symbiont. Science *329*, 212–215.

12. Jiggins, F.M., and Hurst, G.D.D. (2011). Rapid Insect Evolution by Symbiont Transfer. Science *332*, 185–186.

13. Matthews, J.L., Oakley, C.A., Lutz, A., Hillyer, K.E., Roessner, U., Grossman, A.R., Weis, V.M., and Davy, S.K. (2018). Partner switching and metabolic flux in a model cnidarian–dinoflagellate symbiosis. Proceedings of the Royal Society B: Biological Sciences *285*, 20182336.

14. Russell, J.A., and Moran, N.A. (2005). Horizontal Transfer of Bacterial Symbionts: Heritability and Fitness Effects in a Novel Aphid Host. Appl. Environ. Microbiol. *71*, 7987–7994.

15. McGraw, E.A., Merritt, D.J., Droller, J.N., and O'Neill, S.L. (2002). Wolbachia density and virulence attenuation after transfer into a novel host. PNAS *99*, 2918–2923.

16. Nakayama, S., Parratt, S.R., Hutchence, K.J., Lewis, Z., Price, T. a. R., and Hurst, G.D.D. (2015). Can maternally inherited endosymbionts adapt to a novel host? Direct costs of *Spiroplasma* infection, but not vertical transmission efficiency, evolve rapidly after horizontal transfer into *D. melanogaster*. Heredity *114*, 539–543.

17. Sullivan, J.T., Patrick, H.N., Lowther, W.L., Scott, D.B., and Ronson, C.W. (1995). Nodulating strains of Rhizobium loti arise through chromosomal symbiotic gene transfer in the environment. PNAS *92*, 8985–8989.

18. Johnson, M.D. (2011). The acquisition of phototrophy: adaptive strategies of hosting endosymbionts and organelles. Photosynth Res *107*, 117–132.

19. Kadono, T., Kawano, T., Hosoya, H., and Kosaka, T. (2004). Flow cytometric studies of the host-regulated cell cycle in algae symbiotic with green paramecium. Protoplasma *223*, 133–141.

20. Ziesenisz, E., Reisser, W., and Wiessner, W. (1981). Evidence of de novo synthesis of maltose excreted by the endosymbiotic Chlorella from Paramecium bursaria. Planta *153*, 481–485.

21. Kodama, Y., and Fujishima, M. (2011). Four important cytological events needed to establish endosymbiosis of symbiotic *Chlorella* sp. to the alga-free *Paramecium bursaria*. Japanese Journal of Protozoology *44*, 1–20.

22. Siegel, R.W. (1960). Hereditary endosymbiosis in Paramecium bursaria. Experimental Cell Research *19*, 239–252.

23. Sørensen, M.E., Wood, A.J., Minter, E.J., Lowe, C.D., Cameron, D.D., and Brockhurst, M.A. (2020). Comparison of independent evolutionary origins reveals both convergence and divergence in the metabolic mechanisms of symbiosis. Current Biology.

24. Lowe, C.D., Minter, E.J., Cameron, D.D., and Brockhurst, M.A. (2016). Shining a Light on Exploitative Host Control in a Photosynthetic Endosymbiosis. Current Biology *26*, 207–211.

25. Dean, A.D., Minter, E.J.A., Sørensen, M.E.S., Lowe, C.D., Cameron, D.D., Brockhurst, M.A., and Jamie Wood, A. (2016). Host control and nutrient trading in a photosynthetic symbiosis. Journal of Theoretical Biology *405*, 82–93.

26. Minter, E.J.A., Lowe, C.D., Sørensen, M.E.S., Wood, A.J., Cameron, D.D., and Brockhurst, M.A. (2018). Variation and asymmetry in host-symbiont dependence in a microbial symbiosis. BMC Evol Biol *18*, 108.

27. Mallick, N. (2004). Copper-induced oxidative stress in the chlorophycean microalga Chlorella vulgaris: response of the antioxidant system. J. Plant Physiol. *161*, 591–597.

28. Shiu, C.-T., and Lee, T.-M. (2005). Ultraviolet-B-induced oxidative stress and responses of the ascorbate-glutathione cycle in a marine macroalga Ulva fasciata. J. Exp. Bot. *56*, 2851–2865.

29. Kodama, Y., and Fujishima, M. (2008). Cycloheximide Induces Synchronous Swelling of Perialgal Vacuoles Enclosing Symbiotic Chlorella vulgaris and Digestion of the Algae in the Ciliate Paramecium bursaria. Protist *159*, 483–494.

30. Kodama, Y., and Fujishima, M. (2012). Cell division and density of symbiotic Chlorella variabilis of the ciliate Paramecium bursaria is controlled by the host's nutritional conditions during early infection process. Environmental Microbiology *14*, 2800–2811.

31. Cantin, N.E., van Oppen, M.J.H., Willis, B.L., Mieog, J.C., and Negri, A.P. (2009). Juvenile corals can acquire more carbon from high-performance algal symbionts. Coral Reefs *28*, 405.

32. Freeman, C.J., Thacker, R.W., Baker, D.M., and Fogel, M.L. (2013). Quality or quantity: is nutrient transfer driven more by symbiont identity and productivity than by symbiont abundance? The ISME Journal *7*, 1116–1125.

33. Husnik, F., and McCutcheon, J.P. (2016). Repeated replacement of an intrabacterial symbiont in the tripartite nested mealybug symbiosis. PNAS *113*, E5416–E5424.

34. Rolshausen, G., Grande, F.D., Sadowska-Deś, A.D., Otte, J., and Schmitt, I. (2018). Quantifying the climatic niche of symbiont partners in a lichen symbiosis indicates mutualist-mediated niche expansions. Ecography *41*, 1380–1392.

35. Matthews, J.L., Oakley, C.A., Lutz, A., Hillyer, K.E., Roessner, U., Grossman, A.R., Weis, V.M., and Davy, S.K. (2018). Partner switching and metabolic flux in a model cnidarian–dinoflagellate symbiosis. Proceedings of the Royal Society B: Biological Sciences *285*, 20182336.

36. Weis, V.M. (2008). Cellular mechanisms of Cnidarian bleaching: stress causes the collapse of symbiosis. Journal of Experimental Biology *211*, 3059–3066.

37. Abrego, D., Ulstrup, K.E., Willis, B.L., and van Oppen, M.J.H. (2008). Species–specific interactions between algal endosymbionts and coral hosts define their bleaching response to heat and light stress. Proceedings of the Royal Society B: Biological Sciences *275*, 2273–2282.

38. Ye, S., Bhattacharjee, M., and Siemann, E. (2019). Thermal Tolerance in Green Hydra: Identifying the Roles of Algal Endosymbionts and Hosts in a Freshwater Holobiont Under Stress. Microb Ecol *77*, 537–545.

39. Howells, E.J., Beltran, V.H., Larsen, N.W., Bay, L.K., Willis, B.L., and van Oppen, M.J.H. (2012). Coral thermal tolerance shaped by local adaptation of photosymbionts. Nature Climate Change *2*, 116–120.

40. Stein, J.R. (1979). (ED.) Handbook of Phycological Methods: Culture Methods and Growth Measurements (Cambridge University Press).

41. Hoshina, R., Kato, Y., Kamako, S., and Imamura, N. (2005). Genetic Evidence of "American" and "European" Type Symbiotic Algae of Paramecium bursaria Ehrenberg. Plant biol (Stuttg) *7*, 526–532.

42. Schneider, C.A., Rasband, W.S., and Eliceiri, K.W. (2012). NIH Image to ImageJ: 25 years of image analysis. Nature Methods. https://www.nature.com/articles/nmeth.2089.

43. Overy, S.A., Walker, H.J., Malone, S., Howard, T.P., Baxter, C.J., Sweetlove, L.J., Hill, S.A., and Quick, W.P. (2005). Application of metabolite profiling to the identification of traits in a population of tomato introgression lines. J Exp Bot *56*, 287–296.

44. Kanehisa, M., and Goto, S. (2000). KEGG: kyoto encyclopedia of genes and genomes. Nucleic Acids Res. *28*, 27–30.

45. Kanehisa, M., Sato, Y., Furumichi, M., Morishima, K., and Tanabe, M. (2019). New approach for understanding genome variations in KEGG. Nucleic Acids Res. *47*, D590–D595.

46. Smith, C.A., O'Maille, G., Want, E.J., Qin, C., Trauger, S.A., Brandon, T.R., Custodio, D.E., Abagyan, R., and Siuzdak, G. (2005). METLIN: a metabolite mass spectral database. Ther Drug Monit *27*, 747–751.

47. Lenski, R.E., Rose, M.R., Simpson, S.C., and Tadler, S.C. (1991). Long-Term Experimental Evolution in Escherichia coli. I. Adaptation and Divergence During 2,000 Generations. The American Naturalist *138*, 1315–1341.

48. Benton, H.P., Want, E.J., and Ebbels, T.M.D. (2010). Correction of mass calibration gaps in liquid chromatography-mass spectrometry metabolomics data. Bioinformatics *26*, 2488–2489.

49. Smith, C.A., Want, E.J., O'Maille, G., Abagyan, R., and Siuzdak, G. (2006). XCMS: Processing Mass Spectrometry Data for Metabolite Profiling Using Nonlinear Peak Alignment, Matching, and Identification. Anal. Chem. *78*, 779–787.

50. Tautenhahn, R., Böttcher, C., and Neumann, S. (2008). Highly sensitive feature detection for high resolution LC/MS. BMC Bioinformatics *9*, 504.

51. Warnes, G.R., Bolker, B., Bonebakker, L., Gentleman, R., Huber, W., Liaw, A., Lumley, T., Maechler, M., Magnusson, A., and Moeller, S. (2009). gplots: Various R programming tools for plotting data. R package version *2*, 1.

52. Cotton, T.E.A., Pétriacq, P., Cameron, D.D., Meselmani, M.A., Schwarzenbacher, R., Rolfe, S.A., and Ton, J. (2019). Metabolic regulation of the maize rhizobiome by benzoxazinoids. ISME J *13*, 1647–1658.

53. Kaever, A., Lingner, T., Feussner, K., Göbel, C., Feussner, I., and Meinicke, P. (2009). MarVis: a tool for clustering and visualization of metabolic biomarkers. BMC Bioinformatics *10*, 92.

752 54. Caspi, R., Billington, R., Fulcher, C.A., Keseler, I.M., Kothari, A., Krummenacker, M.,
753 Latendresse, M., Midford, P.E., Ong, Q., Ong, W.K., et al. (2018). The MetaCyc
754 database of metabolic pathways and enzymes. Nucleic Acids Res *46*, D633–D639.

755 55. R Core Team (2018). R: A Language and Environment for Statistical Computing.

756 56. Wickham, H. (2016). ggplot2: Elegant Graphics for Data Analysis.

757 57. Pinheiro, J., Bates, D., DebRoy, S., Sarkar, D., and R core Team (2019) (2019). nlme:
758 Linear and Nonlinear Mixed Effects Models.

759

KEY RESOURCES TABLE

REAGENT or RESOURCE	SOURCE	IDENTIFIER
Bacterial and Virus Strains		
Serratia marscesens	Collection of Institut Pasteur	CIP 103235T
Chemicals, Peptides, and Recombinant Proteins		
Protozoan Pellet Media	Carolina Biological Supply	132360
Paraquat dichloride	Sigma-Aldrich	36541; CAS: 75365-73-0
8-peak rainbow calibration particles	BioLegend	422903
Chelex100 resin	Bio-Rad Laboratories	1421253
Deposited Data		
Mass spectrometry, growth rate, fitness assays and flow cytometry data	This paper	DOI: 10.17632/m7tpzttyjx.1
Experimental Models: Organisms/Strains		
P. bursaria – *Chlorella* 186b strain	Culture Collection of Algae and Protozoa	CCAP 1660/18
P. bursaria – *Chlorella* HA1 strain	National BioResource project	NBRP ID: PB034004A
P. bursaria – *Chlorella* HK1 strain	National BioResource project	NBRP ID: PB033003A
Oligonucleotides		
primer ‘SR1’ (F): TACCTGGTTGATCCTGCCAG	[41]	N/A
Primer ‘CHspeRmaeF’ (F): GGGCCTTTTCAGGTCTGGTA	[41]	N/A
Primer ‘INT4F’: TGGTGAAGTGTTCGGATTGG	[41]	N/A
Primer ‘SR8’ (F): GGATTGACAGATTGAGAGCT	[41]	N/A
Primer ‘chSsotoR’: CCCTCTAAGAAGTCCGCCG	[41]	N/A
Primer ‘INT5R’: AGGTGGGAGGGTTTAATGAA	[41]	N/A
Primer ‘HLR3R’: TCCCAAACAACCCGACTCT	[41]	N/A
Primer ‘TreSR’: GCCAGTGCACACCGAAAC	[41]	N/A

Primer ‘CHspeHLR1R’: CACTAGACTACAATTCGCCAGCC	[41]	N/A
Software and Algorithms		
Visual Basic macro 216	[43]	https://pubmed.ncbi.nlm.nih.gov/15596481/
ImageJ v1.50i	[42]	https://imagej.nih.gov/ij/
xcms R package	[48–50]	https://bioconductor.org/packages/release/bioc/html/xcms.html
MarVis-Suite 2.0 software	[53]	http://marvis.gobics.de/

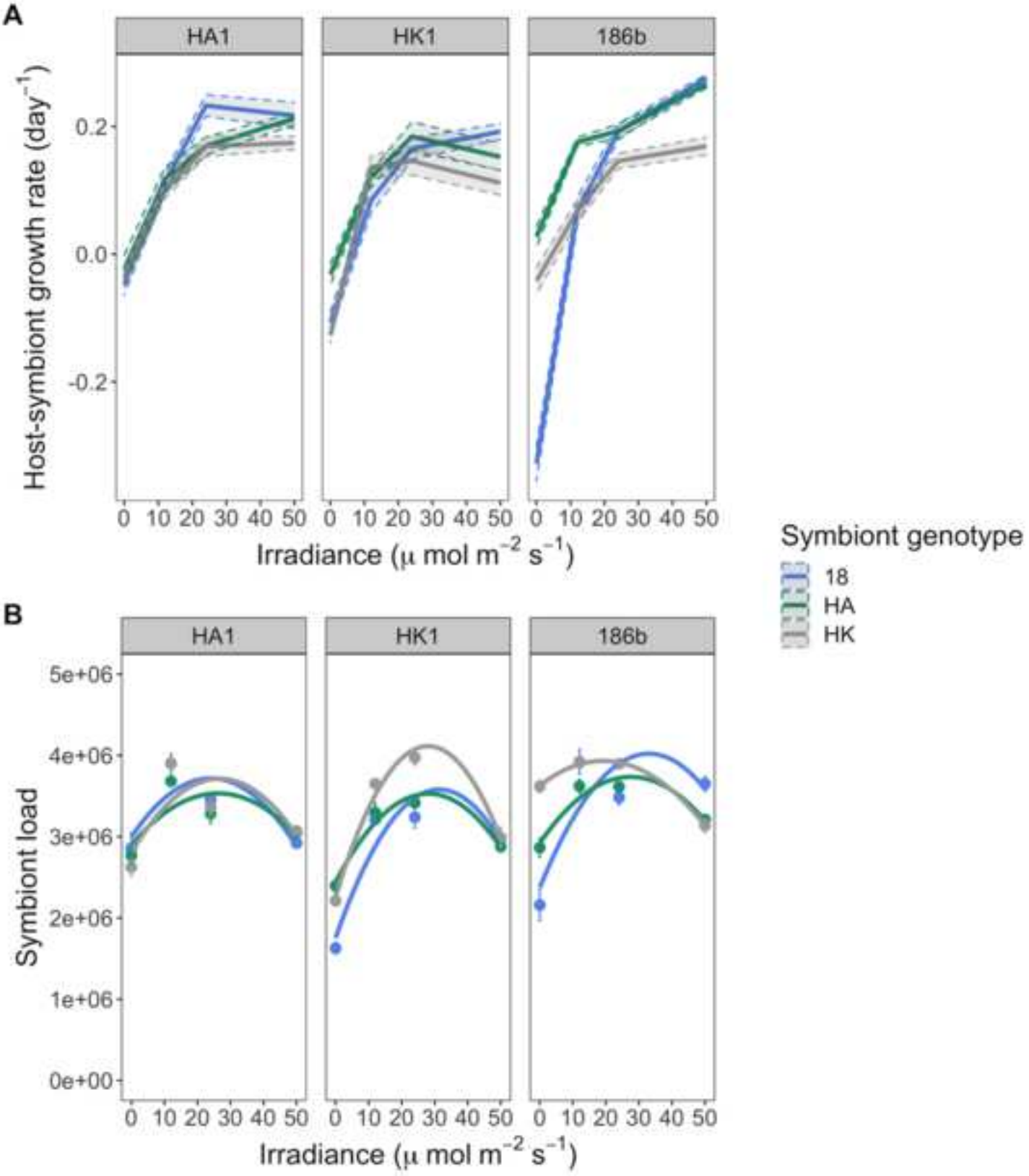

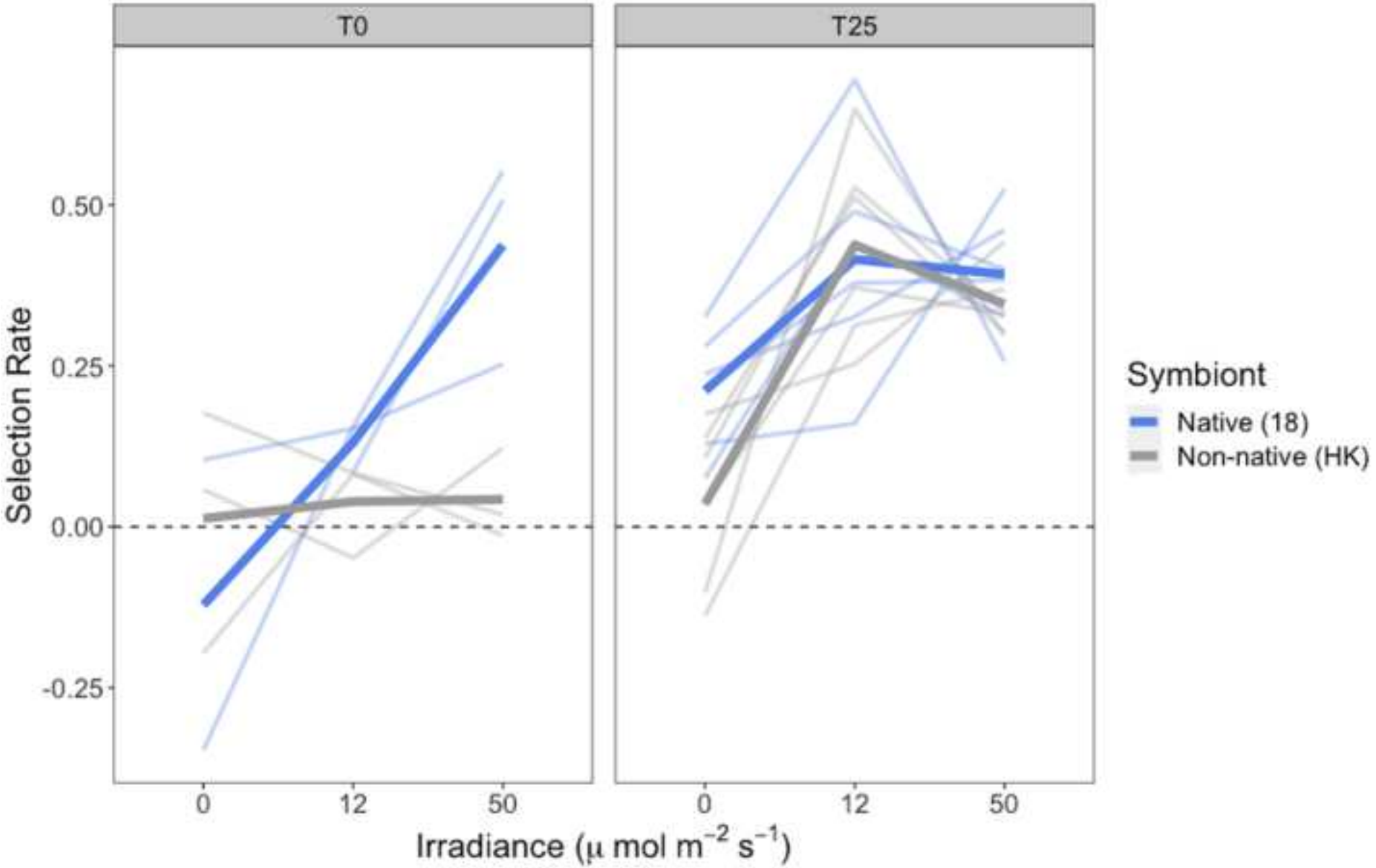

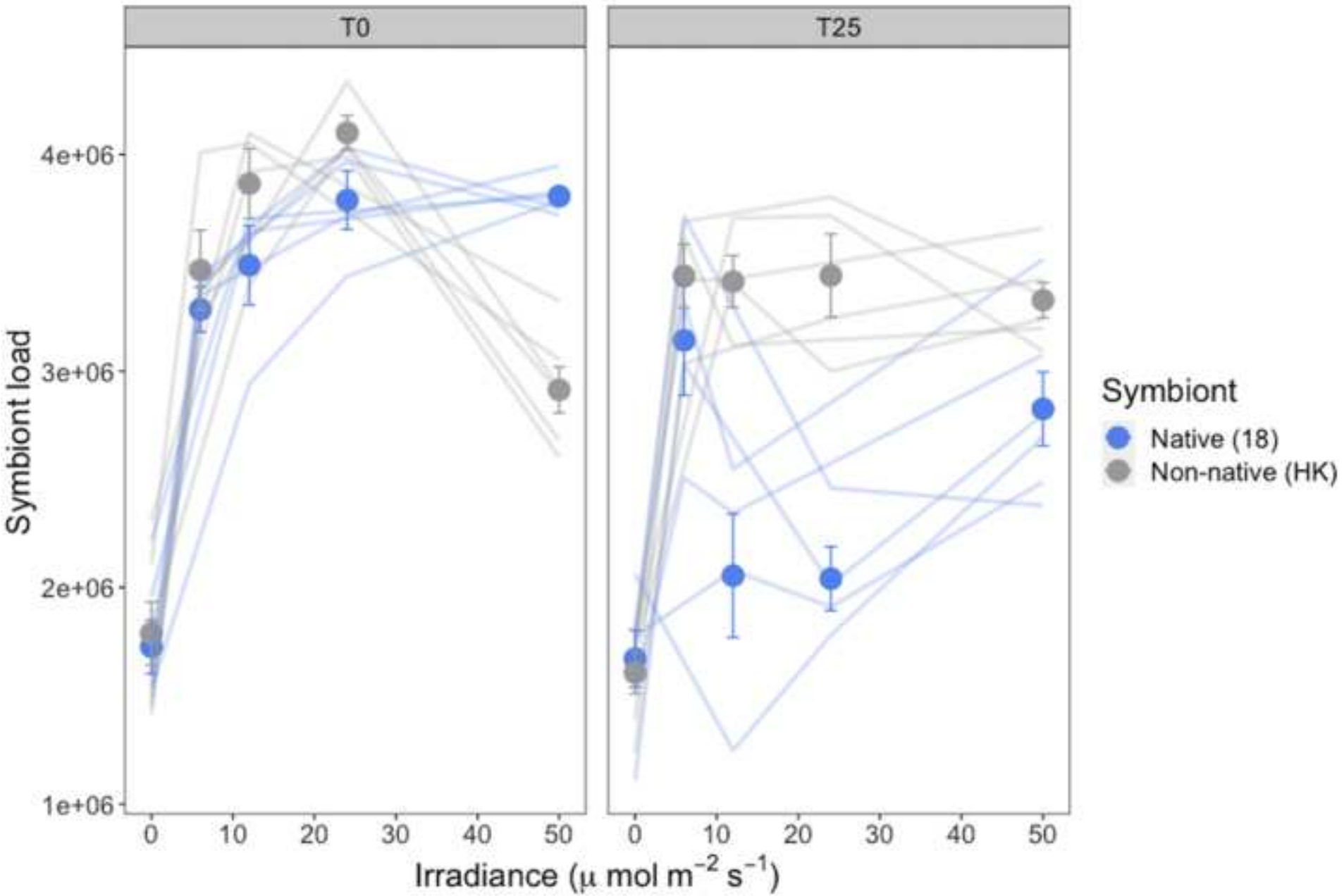

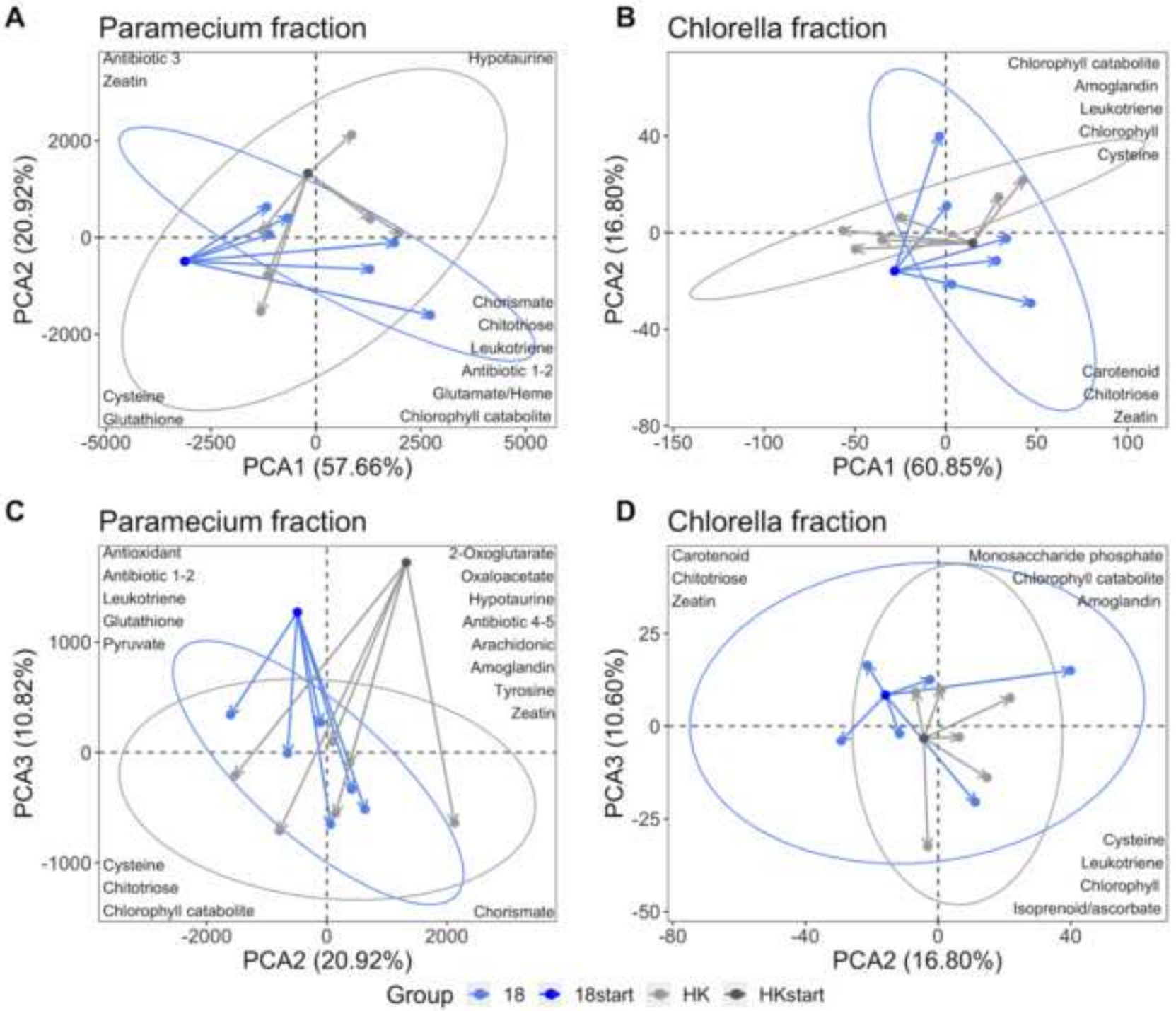

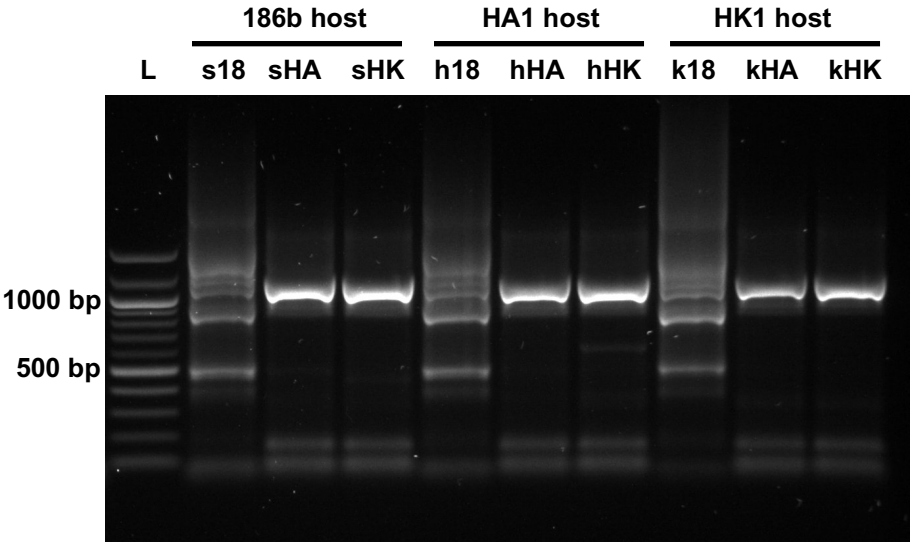

Figure S1. PCR confirmation of symbiont-genotype within the reciprocal cross infections. Related to STAR Methods and main text.
Overlapping, multiplex primers were used to amplify fragments within the 18S rDNA and ITS region of the *Chlorella* nuclear genome. In this region the 'American/Japanese' strains, such as HA1 and HK1, have had three introns inserted that the 'European' strains, such as 186b, lack (Hoshina and Imamura, 2008; Hoshina et al., 2005). The banding pattern results here confirm that the cross-infections were successful and contain the correct *Chlorella* genotype, specifically that the distinct banding pattern of 186b was present when expected. This PCR method can distinguish between 'American/Japanese' and 'European' strains, but not between strains that come from the same biogeographical clade. Host genotype has been shortened to a letter ('s' = 186b host, 'h' = HA1 host, 'k' = HK1 host); symbiont genotype is shown by two capitals ('18' = 186b symbiont, 'HA' = HA1 symbiont, 'HK' = HK1 symbiont. Shown alongside a 100bp ladder.

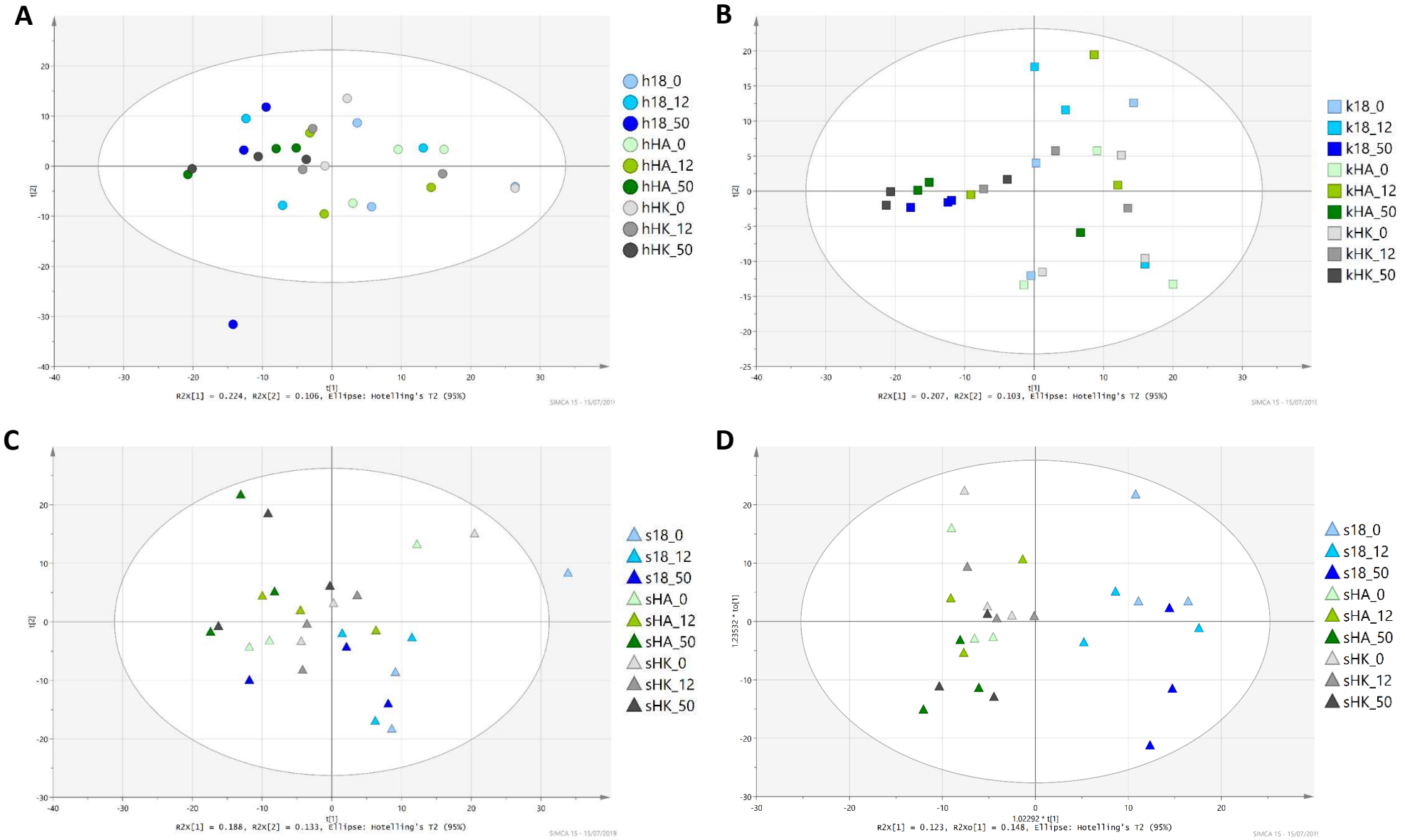

Figure S2. Clustering patterns of the *Chlorella* metabolic fraction subset by host-genotype. Related to the main text.
Plots A-C are PCA plots and show the HA1 host (A), the HK1 host (B), and the 186b host (C). Each point represents the metabolic profile of a sample; with the shape denoting the *P. bursaria* host genotype, the colour denoting the *Chlorella* symbiont genotype and the colour shade denoting the light intensity. Only within the 186b host (C) do the samples clusters by colour, and therefore, symbiont genotype. Following this initial clustering, the 186b host subset was subject to OPLS-DA (D). Here the samples separate between the 'blue' samples (186b symbiont-genotype) and the 'green' and 'grey' samples (HA1 and HK1 symbiont genotypes). There are 3 replicates of each combination of host, symbiont and light intensity.

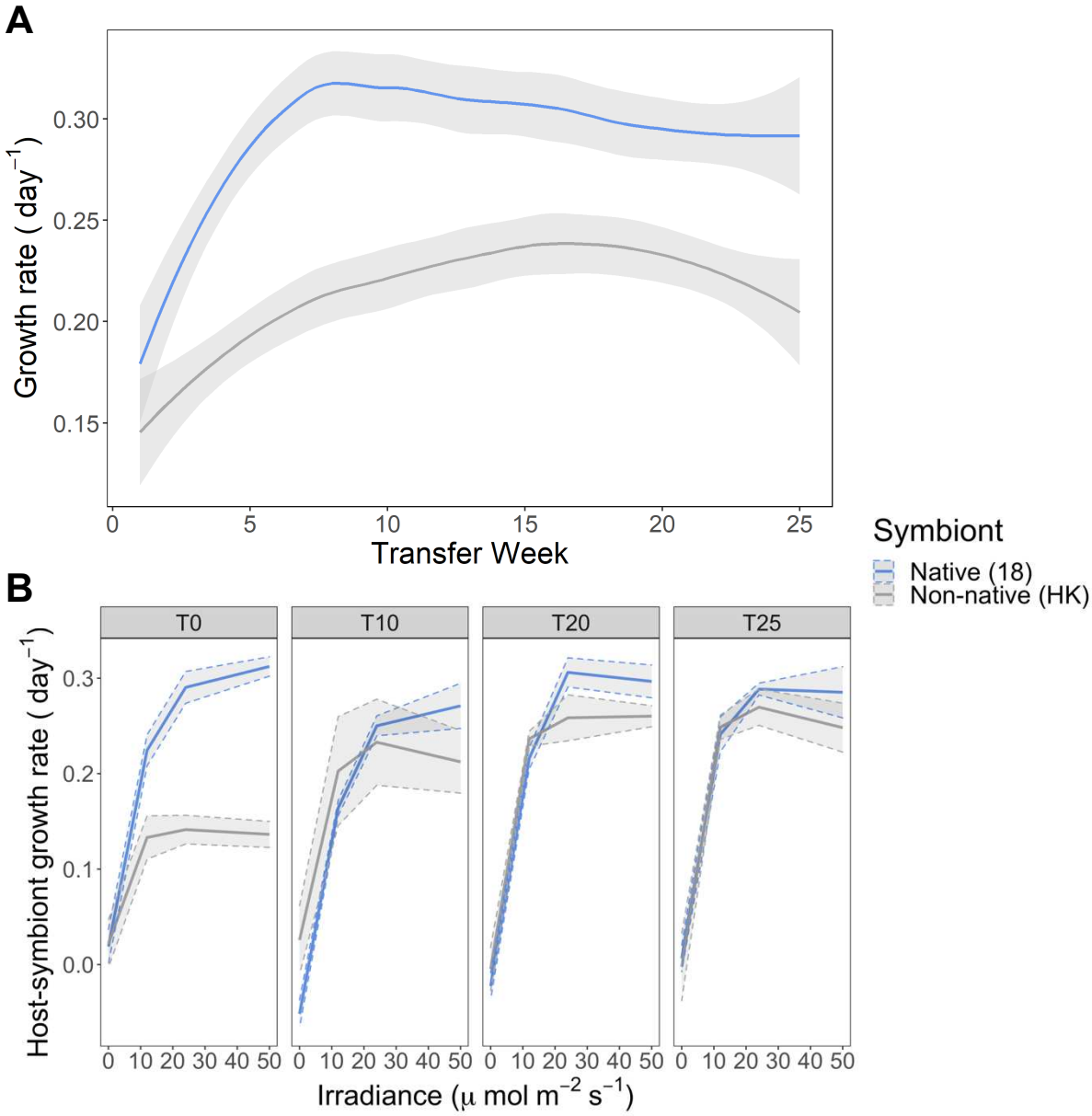

Figure S3. Growth rate across and within the evolution experiment. Related to the main text.

The weekly growth rate of the native and novel symbioses across the experiment are shown in plot A. The lines show the smoothed mean (n=6) growth rates ± SE. The smoothing function used was the loess method. Over the course of the experiment, the growth rate with either symbiont increases, though the growth rate with the native symbiont was consistently higher than with the non-native symbiont. Plot B depicts the growth rate assays performed at multiple points throughout the experiment. Each panel shows the mean (n=6) initial growth rate measured over three days across a light gradient and the shaded area denotes ± SE. The panels represent the transfer week within the evolution experiment at which the growth assay was performed (T0 = week 0, T10 = week 10, T20 = week 20 & T25 = week 25). At the start of the evolution experiment, there was a difference between the growth rates with the native compared to the non-native symbiont at high light, over the course of the experiment this difference disappeared. In both plots colour denotes the symbiont genotype within the 186b host.

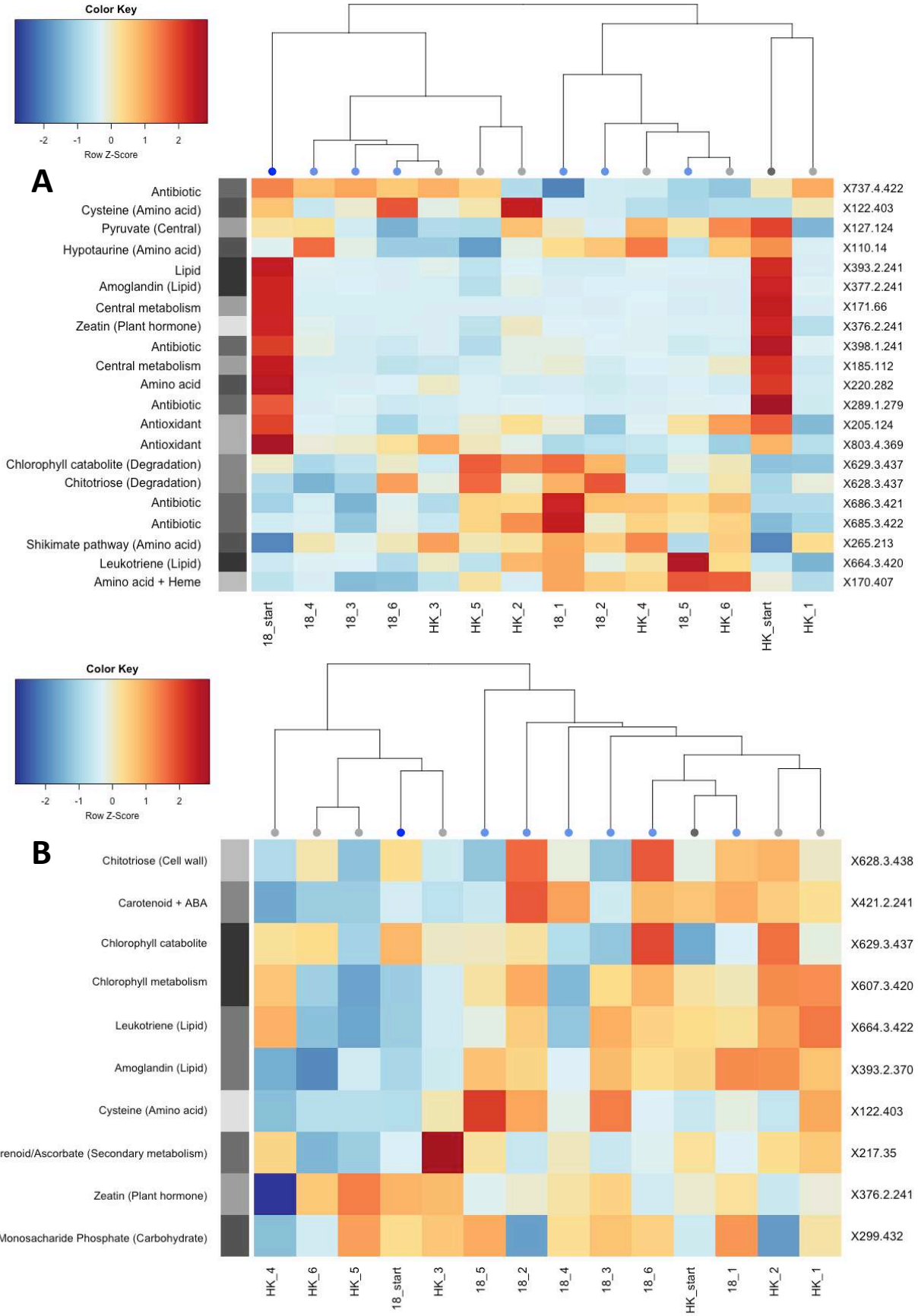

Figure S4. Metabolites of interest across the start and end of the evolution experiment. Related to Figure 4 and the main text.

The *P. bursaria* metabolic fraction is shown in A and the *Chlorella* fraction in B. The data is presented as heatmaps with colour representing the relative abundance of the metabolites. The metabolites depicted were identified from the top loadings of the PCA plots. The columns in the heatmap correspond to sample; these are labelled with their symbiont-genotype (18 = 186b; HK = HK1) and with the replicate number if from the end of the experiment or 'start' if from the start. The column on the left of the heatmap indicates the compound/functional group of the metabolites and the column on the right indicates the loading ID, which corresponds to the identification Table S3. The phylogeny of the samples was calculated with their principal component coordinates using UPGMA clustering, and the order of the rows was assigned by UPGMA clustering performed on the rows' distance measures (based on the Pearson correlation co-efficient).

Table S2 Symbiont-genotype specific metabolites within the 186b *P. bursaria* host. Related to the main text. These metabolite IDs were highlighted by the pairwise contrasts and were found to have significantly higher abundances in one symbiont-genotype compared to another within the 186b host subset of the *Chlorella* metabolic fraction in the dark (0µE) and in the highest light condition (50µE).

Light Condition	Strain associated	Comparison	mz ID	Detected mass	Accurate mass	Adduct	Candidate Compound	Pathway	Stress Associated
0µE	**s18**	s18 vs sHA	118	117.966	117.0426	H+	Aspartate-4-semialdehyde	Amino acid	
					117.0578	H+	Indole	Amino acid + hormone	
					117.0790	H+	Glycinebetaine	Amino acid + osmolyte	
					117.0790	H+	Valine	Amino acid	
		s18 vs sHA	134.2	134.109	133.1040	H+	Aspartate	Amino acid	
		s18 vs sHA	255.2	255.104	216.1725	K+	w-hydroxydodecanoic acid	Hydroxy fatty acids	
					254.2246	H+	Palmitoleic acid	Unsaturated fatty acids	
		s18 vs sHA	343.2	343.153	342.1162	H+	Disaccaride	Carbohydrate	
					304.2402	K+	Arachidonic acid	Unsaturated fatty acids	Yes
					304.2402	K+	Kaurenoic acid	Diterpenoid (related to GA)	
		s18 vs sHK	247.2	247.117	224.1412	Na+	Methyl jasmonate	Hormone (JA)	Yes
		s18 vs sHK	267.2	267.102	228.2089	K+	Myristic acid	Saturated fatty acids	
					244.2263	Na+	N1-acetylspermine	Amino acid	
		s18 vs sHK	271.2	271.167	248.1412	Na+	Abscisic acid aldehyde	Hormone (ABA)	Yes
		s18 vs sHK	686.4	686.391	663.3748	Na+	1-Palmitoyl-2-(5-keto-6-octenedioyl)-sn-glycero-3-phosphocholine	Glycerophospholipids	Yes
	sHK	s18 vs sHK	220.2	220.153	219.1107	H+	Pantothenate	Vitamin (B5)	
					219.1120	H+	Zeatin	Hormone (cytokinin)	
		s18 vs sHK	238	238.053	199.0246	K+	O-phospho-L-homoserine	Amino acid	
					215.0195	Na+	O-phospho-4-hydroxy-L-threonine	Vitamin (B6)	
					215.0807	Na+	Kinetin	Hormone (cytokinin)	
		s18 vs sHK	241.2	241.188	202.2157	K+	Spermine	Amino acid	
		s18 vs sHK	335.2	335.115	334.2144	H+	Prostaglandin	Fatty acyls	
					312.3028	Na+	Eicosanoic acid	Saturated fatty acids	
	sHK	sHA vs sHK	355	355.048	354.0577	H+	5-amino-(5'-phosphoribosylamino)uracil	Riboflavin	

Table S2 continued

Light Condition	Strain associated	Comparison	mz ID	Detected mass	Accurate mass	Adduct	Compound	Pathway	Stress Associated
50µE	**s18**	s18 vs sHA	171	171.088	132.0059	K+	Oxalacetic acid	TCA /central	
					169.9980	H+	Glycerone phosphate	Glycolysis / central	
					169.9980	H+	Glyceraldehyde-3-phosphate	Glycolysis / central	
					132.0423	K+	3-hydroxy-3-methyl-2-oxobutanoate	Amino acid	
					132.0423	K+	2-acetolactate	Amino acid	
					132.0423	K+	Glutarate	Amino acid	
					132.0535	K+	Asparagine	Amino acid	
					148.0372	Na+	Citramalate	C5-Branched dibasic acid	
					132.0899	K+	Ornithine	Amino acid	
					148.0736	Na+	Mevalonic acid	Mevalonate pathway	
					148.0736	Na+	Pantoate	Pantothenate biosynthesis	
		s18 vs sHA	237.2	237.181	214.1317	Na+	Dethiobiotin	Vitamin (B7)	
		s18 vs sHA	239.2	239.145	200.1776	K+	Lauric acid	Saturated fatty acids	
					216.1725	Na+	w-hydroxydodecanoic acid	Hydroxy fatty acids	
		s18 vs sHA	251.2	251.146	228.2089	Na+	Myristic acid	Saturated fatty acids	
					212.2504	K+	Pentadecane	Hydrocarbon	
		s18 vs sHA	537.4	537.356	536.4382	H+	α/β/γ/δ carotene	Carotenoid	
					536.4382	H+	Lycopene (all-trans or tetra cis)	Carotenoid	
		s18 vs sHK+sHA	213	213.097	174.0164	K+	Aconitic acid	TCA cycle / central	
					190.0114	Na+	Oxalosuccinate	TCA cycle / central	
					174.0528	K+	3-Carboxy-4-methyl-2-oxopentanoate	Amino acid	
					174.0528	K+	Shikimic acid	Shikimate pathway	
					190.0477	Na+	3-dehydroquinate	Shikimate pathway	
					174.0793	K+	Indole-3-acetamide	Amino acid + hormone	
					174.0892	K+	Suberic acid	Fatty acid	
					174.1004	K+	N2-acetyl-L-ornithine	Amino acid	
					190.1066	Na+	y-hydroxy-l-arginine	Arginine-nitric oxide	
					212.0896	H+	Volemitol	Carbohydrate	

Table S2 continued

Light Condition	Strain associated	Comparison	mz ID	Detected mass	Accurate mass	Adduct	Compound	Pathway	Stress Associated
50µE	**s18**	s18 vs sHK+sHA	257.2	257.123	256.2402	H+	palmitic acid	saturated fatty acid	
					256.1172	H+	2-(3-Carboxy-3-aminopropyl)-L-histidine	unusual amino acid	
		s18 vs sHK	235.2	235.131	212.2504	Na+	pentadecane	Hydrocarbon - metabolite	
	sHK	s18 vs sHK	220.2	220.153	219.1120	H+	Zeatin	Hormone	
					219.1107	H+	Pantothenate	vitamin B5	
	sHK + sHA	s18 vs sHK+sHK	465	465.096	426.0879	K+	S-Glutathionyl-L-cysteine	Cysteine + methionine	Yes
	sHK	sHA vs sHK	329.2	329.178	328.2402	H+	Docosahexaenoic acid	Unsaturated fatty acids	

Table S3. Identified metabolites associated with PCA trajectories for the *P. bursaria and Chlorella* fraction in the evolution experiment. Related to Figure 4 and the main text. These were identified from the top 1% of loadings when using the first three principal components. The metabolite ID is that referred to in Figure 4.

Fraction	PC of loading	ID	Detected mass	Accurate mass	Adduct	Function	Pathway	Compound	Kegg / Metacyc
P. bursaria	PC1,3	X110.14	110	109.0197	H+	Amino acid	Taurine metab	Hypotaurine	C00519
	PC1	X170.407	170	131.0582	K+	Amino acid+Heme	Heme biosynthesis	5-Amino-4-oxopentanoate	C00430
				147.0532	Na+		Amino acid/Central	Glutamate	C00025
				131.0582	K+		Amino acid	Glutamate 5-semialdehyde	C01165
	PC1,2,3	X265.213	265	226.0477	K+	Amino acid	Shikimate pathway	Chorismate	C00251
				226.0477	K+		Shikimate pathway	Prephenate	C00254
				242.0192	Na+		Shikimate pathway	Deoxy-ketofructose-phosphate	C16848
	PC1,2,3	X376.2.241	376.2	353.1699	Na+	Plant hormone	Plant hormone (zeatin)	Dihydrozeatin riboside	C16447
	PC1,2,3	X628.3.437	628.3	627.2487	H+	Plant degradation	Chitin degradation	Chitotriose	CPD13227
	PC1, 2	X629.3.437	629.3	628.2897	H+	Plant degradation	Chlorophyll degradation	Chlorophyll catabolite	C18098
	PC1, 2	X664.3.420	664.3	625.3033	K+	Lipid	Lipid - Arachidonic acid	Leukotriene C4	C02166
	PC1,2,3	X685.3.422	685.3	684.3178	H+	Antibiotic	Antibiotic	gamma-L-Glutamyl-butirosin B	C18005
	PC1, 2	X686.3.421	686.3	685.3256	H+	Antibiotic	Antibiotic	Viomycin	C01540
	PC1	X737.4.422	737.4	714.3979	Na+	Antibiotic	Antibiotic	Avermectin B1b monosaccharide	C11965
	PC1,3	X803.4.369	803.4	780.3622	Na+	Antioxidant	Glutathione metabolite	Bis(glutathionyl)spermine	C16563
	PC2	X122.403	122	121.0197	H+	Amino acid	Amino acid	Cysteine	C00736
	PC3	X127.124	127	88.0160	K+	Central	TCA/Glycolysis	Pyruvate	C00022
				104.0110	Na+		Amino acid	Hydroxypyruvate	C00168
	PC3	X171.66	171	132.0059	K+	Central	Central/TCA/Glycolysis	Oxaloacetate	C00036
				169.9980	H+		Glycolysis/Carbohydrate	Glycerone phosphate	C00111
				169.9980	H+		Glycolysis/Carbohydrate	Glyceraldehyde 3-phosphate	C00118
				132.0535	K+		Amino acid	L-Asparagine	C00152
	PC3	X185.112	185	146.0215	K+	Central	Central/TCA/amino acids	2-Oxoglutarate	C00026
				146.0579	K+		Pantothenate + CoA	2-Dehydropantoate	C00966
				146.0579	K+		Amino acid	2-Aceto-2-hydroxybutanoate	C06006
	PC3	X205.124	205	182.0579	Na+	Antioxidant	Amino acid/antioxidant	4-Hydroxyphenyllactate	C03672
				182.0215	Na+		Antibiotic	3;5-Dihydroxyphenylglyoxylate	C12325
				166.0491	K+		Purine alkaloid	Methylxanthine	C16353

Table S3 continued

Fraction	PC of loading	ID	Detected mass	Accurate mass	Adduct	Function	Pathway	Compound	Kegg / Metacyc
P. bursaria	PC3	X220.282	220	181.0739	K+	Amino acid	Amino acid	Tyrosine	C00082
				181.0739	K+		Amino acid	N-Hydroxy-L-phenylalanine	C19712
	PC3	X289.1.279	289.1	288.0998	H+	Antibiotic	Antibiotic	6-Deoxydihydrokalafungin	C12435
	PC3	X377.2.241	377.2	354.2406	Na+	Lipid	Lipid - Arachidonic acid	Amoglandin	C00639
	PC3	X393.2.241	393.2	354.2406	K+	Lipid	Lipid - Arachidonic acid	Amoglandin	C00639
				370.2355	Na+		Lipid - Arachidonic acid	6-Keto-prostaglandin F1alpha	C05961
				370.2355	Na+		Lipid - Arachidonic acid	Thromboxane B2	C05963
	PC3	X398.1.241	398.1	359.1151	K+	Antibiotic	Antibiotic	Penicillin N	C06564
				397.0798	K+		Antibiotic	4-Ketoanhydrotetracycline	C06627
Chlorella	PC1,2,3	X122.403	122	121.0197	H+	Amino acid	Amino acid	Cysteine	C00097
	PC1, 3	X393.2.370	393.2	354.2406	K+	Lipid	Arachidonic acid	Amoglandin	C00639
				370.2355	Na+		Arachidonic acid	6-Keto-PGF1a	C05961
				370.2355	Na+		Arachidonic acid	Thromboxane B2	C05963
	PC1, 2	X421.2.241	421.2	382.2508	K+	Carotenoid + ABA	Carotenoid+ABA synthesis	C25-Allenic-apo-aldehyde	C14044
	PC1, 3	X628.3.438	628.3	627.2487	H+	Cell wall metab	Chitin degradation	Chitotriose	CPD13227
	PC1, 3	X629.3.437	629.3	628.2897	H+	Chlorophyll degradation	Chlorophyll degradation	Chlorophyll catabolite	C18098
	PC1,2,3	X664.3.422	664.3	625.3033	K+	Lipid	Arachidonic acid	Leukotriene C4	C02166
	PC2, 3	X376.2.241	376.2	353.1699	Na+	Plant hormone	Plant hormone (Zeatin)	Dihydrozeatin riboside	C16447
	PC2	X607.3.420	607.3	568.305	K+	Chlorophyll	Chlorophyll metabolism	Protoporphyrinogen IX	C01079
				584.2635	Na+		Chlorophyll metabolism	Bilirubin	C00486
	PC3	X217.35	217	178.0477	K+	Secondary metabolite	Ascorbate/Vitamin C	L-Galactono-1;4-lactone	C01115
				194.0579	Na+		Phenylpropanoid/cell walls	Ferulate	C01494
				216.0399	H+		Isoprenoid biosynthesis	2-Methylerythritol 4-phosphate	C11434
				178.063	K+		Phenylpropanoid/cell wall	Coniferaldehyde	C02666
	PC3	X299.432	299	260.0297	K+	Monosaccharide	Starch + sucrose	Glucose 6-phosphate	C00092
				260.0297	K+	Phosphate	Glycolysis	Glucose 1-phosphate	C00103
				260.0297	K+		Fructose and mannose	Mannose 6-phosphate	C00275
				276.0246	Na+		Pentose phosphate	6-Phospho-D-gluconate	C00345
				260.0297	K+		Galactose	Galactose 1-phosphate	C00446
				260.0297	K+		Fructose and mannose	Mannose 1-phosphate	C00636

Table S4. Change in symbiont load for each HK1 replicate between the start and end of the evolution experiment. Related to the main text.
The metabolic group column denotes whether the replicate's metabolic profile appeared converged with the profile of the native 186b symbionts or diverged. From these two groups ('converge' or 'diverge') a group mean difference in symbiont load was calculated.

HK1 replicate	Difference in symbiont load	Metabolic trajectory appeared to	Mean difference in symbiont load
1	145404.2	converge	
2	337137.9	converge	241271
3	745804.2	diverge	
4	426775.4	diverge	
5	490066.7	diverge	500951.4
6	341159.3	diverge	